Helium nano-bubble bursting near the nickel surface*

Heng-Feng Gong(龚恒风)[1,2,3,4,†], Min Liu(刘敏)[2], Fei Gao(高飞)[4], Rui Li(李锐)[1], Yan Yan(严岩)[1], Heng Huang(黄恒)[1], Tong Liu(刘彤)[1], and Qi-Sen Ren(任啟森)[1]

[1] *ATF R&D Accident Tolerant Fuel Research and Development, China Nuclear Power Technology Research Institute Co., Ltd, Shenzhen* 518000, *China*
[2] *Shanghai Institute of Applied Physics, Chinese Academy of Sciences, Division of Nuclear Materials and Engineering, Shanghai* 201800, *China*
[3] *Key Laboratory of Interfacial Physics and Technology, Chinese Academy of Sciences, Shanghai* 201800, *China*
[4] *Department of Mechanical Engineering, University of Michigan, Ann Arbor, Michigan* 48109, *USA*

(Received 1 June 2017; revised manuscript received 19 July 2017; published online 29 September 2017)

We have investigated the expansion and bursting of a helium nano-bubble near the surface of a nickel matrix using a molecular dynamics simulation. The helium atoms erupt from the bubble in an instantaneous and volcano-like process, which leads to surface deformation consisting of cavity formation on the surface, along with modification and atomic rearrangement at the periphery of the cavity. During the kinetic releasing process, the channel may undergo the "open" and "close" states more than once due to the variation of the stress inside the nano-bubble. The ratio between the number of helium atoms and one of vacancies can directly reflect the releasing rate under different temperatures and crystallographic orientation conditions, respectively. Moreover, a special relationship between the stress and He-to-vacancy ratio is also determined. This model is tested to compare with the experimental result from Hastelloy N alloys implanted by helium ions and satisfactory agreement is obtained.

Keywords: molecular dynamics, nano-bubbles, near surface

PACS: 34.10.+x, 36.40.Sx, 68.03.Cd **DOI:** 10.1088/1674-1056/26/11/113401

1. Introduction

The formation of helium bubbles leads to high-temperature intergranular embrittlement, which eventually leads to the degradation of the mechanical integrity of materials,[1,2] and then affects the lifetime and the safety of the reactor at some level. The Hastelloy N alloys as the structural material in the molten salt reactor (MSR) contain 68% ^{58}Ni (nickel, Ni) and 26% ^{60}Ni, both of which can generate helium (He) by the (n, α) transmutation reaction, as follows: $58\text{Ni} + n_{\text{f}} \rightarrow 55\text{Fe} + 4\text{He}$ and $60\text{Ni} + n_{\text{f}} \rightarrow 57\text{Fe} + 4\text{He}$. An estimated 40 ppm of helium was generated in molten salt breeder reactor (MSBR) over 30 years.[3] Liu *et al.*[4] described the surface blistering and cracking phenomenon experimentally on Hastelloy N alloys implanted with 30-keV helium ions and doses of 1×10^{15}, 5×10^{15}, and 1×10^{16} He/cm^2 respectively, and the temperature is 500 °C. The mean range of the implanted helium was 240 nm and the irradiation area is around 200 nm, while for the peak value the irradiation is about 100 nm. The study suggested that the observation of surface blistering and the nano-bubble sizes phenomenon are within the range from 0.5 to 3.0 μm. The distribution and size of nano-bubble are not uniform, rather than alignment or aggregation. Of interest here were the results which showed in the implanted area the single nano-bubble is mainly sphere and even the outline of the capped nano-bubble forms as shown in Ref. [4], and the nano-bubble breakups and the cracks appear on the surface randomly as the dose increases.

The formation of gas-filled blisters in the surface region of irradiated solids has been also observed.[5–7] The blisters can rupture in energetically favored regions and thereby release bursts of gas. Blistering plays a very important role in issue about helium embrittlement, since it can lead to (i) serious damage and erosion of bombarded surfaces and (ii) the release of gases which will contaminate the secondary circuit. Much experimental research about the behavior of He nano-bubble in metals has been carried in recent decades.[8–12] For instance, Cipiti *et al.*[12] implanted helium and deuterium into polished tungsten specimens under high temperature. They analyzed the effects of the energy of the incident ion beam and temperature on the surface structures. Zenobia *et al.*[13] studied that the retention and surface pore formation with 30 keV ^{3}He implanted into tungsten at temperatures ranging from 850–1000 °C. The results indicated that the threshold for the surface pore formation occurs between $\sim 5 \times 10^{16}$–4×10^{17} He$^+$/cm^2 and with the higher implanted influence, both surface and sub-surface pore formation is also observed to increase. Generally, the gas driven model and the lateral stress driven model are used to explain the mechanism of blistering on the surface. For example, Sefta *et al.*[14,15] investigated the bursting behavior of sub-surface, helium bub-

*Project supported by the Program of International Science and Technology Cooperation of China (Grant No. 2014DFG60230), the National Basic Research Program of China (Grant No. 2010CB934504), the Strategically Leading Program of the Chinese Academy of Sciences (Grant No. XDA02040100), the Shanghai Municipal Science and Technology Commission, China (Grant No. 13ZR1448000), and the National Natural Science Foundation of China (Grant Nos. 91326105 and 21306220).

†Corresponding author. E-mail: gonghengfeng@cgnpc.com.cn

© 2017 Chinese Physical Society and IOP Publishing Ltd

bles pressure evolution and the resulting tungsten surface morphology. Their results provided insight into the conditions and mechanisms leading to various tungsten topology changes and surface roughening occurs as single adatoms migrate to the surface, prismatic loops glide to the surface to form islands, and ultimately as over-pressurized helium bubbles burst. Zhang *et al.*[16] studied helium bubble formation and releasing near the titanium surface. Their results suggest that the helium bubble burst results in pores in the metal surface and the size of the resultant surface pore depends on the initial bubble diameter. Ohno *et al.*[17] have investigated that the influence of crystallographic orientation on the formation of helium bubble and nanostructure by using ITER grade tungsten (W) exposed to helium plasma. The helium bubbles with a large helium pressure move the W lattice along the slip face. El-Atwani *et al.*[18] observed that the largest bubbles were formed on the grain boundaries, and future work will focus on the bubble coalescence and the effect of grain orientation. Though there has been much research about the helium bubble releasing near the metal surface, there are still problems left behind, such as, how the orientation affects the helium nano-bubble releasing and how the environment temperature and He-to-vacancy ratios affect the releasing process of helium bubble from the metal surface and even the stress variants in the complete releasing process.

In the present work, we investigated the evolution of helium nanobubbles near the nickel surface in terms of the variation of orientations, helium-to-vacancy ratios, temperatures and release mechanisms involved at the atomic level to provide a reasonable picture of the blistering formation and gas release results reported by Liu *et al.*[4]

2. Methodology

All calculations were performed using the molecular dynamics (MD) simulation with the atomic/molecular massively parallel simulator (LAMMPS) software package.[19] The atomic interactions of Ni–Ni, Ni–He, and He–He atoms were described by the modified analytic EAM model (MAEAM),[20–29] the Morse potential,[30] and the Lennard–Jones potential,[22] respectively. More information about the formulas and parameters can be found in Ref. [32]. Periodic boundary conditions were applied in the X- and Y-directions, while the Z-direction was a free surface. The $[001]$, $[1-10]$, and $[111]$ single crystal surfaces were considered to be the helium nano-bubble releasing paths, respectively. To present the atoms moving in the vertical direction due to the escape of helium atoms, the bottom three layers of the simulation box were frozen in the simulation process.

Three-dimensional periodic computational cell of $12a_0 \times 12a_0 \times 12a_0$ was used to eliminate surface effects, where a_0 is the lattice constant of face-center cubic nickel crystal ($a_0 = 3.5157$ Å). The temperature was set to 300 K, 500 K, 800 K, and 1000 K, respectively. The Nosé–Hoover style non-Hamitonian equation of motion describes the constant temperature technique[33] with a time step of 0.5 femtosecond (fs). The helium-to-vacancy ratios were 1 : 0, 2 : 1, 3 : 1, and 4 : 1, respectively. The Polak–Ribiere version of the conjugate gradient (CG) algorithm was used to relax the whole simulation systems.[33] There was no pressure control in the whole simulation process. The total simulation time was 600.0 picosecond (ps). The equilibrium helium nano-bubble was created by moving a certain nickel volume to initially form a spherical void with a radius of 8.0 Angstrom (Å) and then inserting helium atoms for the specific ratio with vacancies into it at once. We only considered a spherical helium bubble with a radius of 7.0 Å to ensure the stability of helium nano-bubble for modelling. Furthermore, the depth (H) of the helium nano-bubble from the surface to the mass center of bubble will influence on the pressure of nano-bubble, and the behavior of nano-bubble releasing process. Here, we only considered the critical depth (H) which can exactly satisfy the pressure of nano-bubble releasing. In different initial conditions, such as temperature, helium-to-vacancy ratio, and single crystal free surface, the depth (H) needs to be adjusted to make the releasing process just appear. The sketch is shown in Fig. 1, in which the atomic arrangement is given to help understand the nano-bubble bursting and escaping process from the free surface.

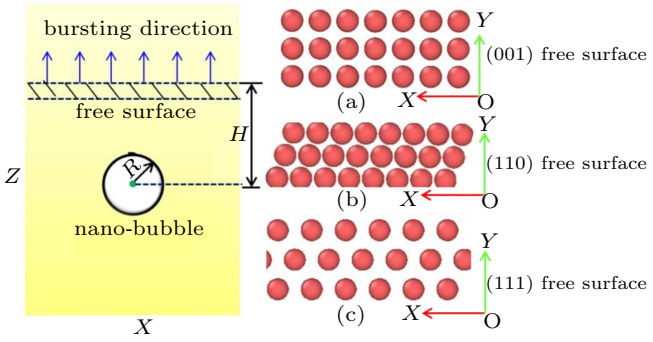


Fig. 1. (color online) The sketch for nano-bubble bursting near the different crystal free surfaces: (a) (001) free surface; (b) (110) free surface; (c) (111) free surface.

3. Results and discussion

3.1. The effect of different variables on the behavior of helium nano-bubble escaping

Due to the limitation of experimental observation, it is very important to understand the evolution and release behavior of helium nano-bubbles near the crystalline surface and the corresponding mechanisms by simulation means. To illuminate the effect of crystallographic orientations on the behavior of the helium nano-bubbles, we simulated three crystallographic orientations, such as $[001]$, $[1-10]$, and $[111]$, which are along the escaping direction of the helium nano-bubbles.

For the three free surface orientations, the releasing process of helium nano-bubbles can be mainly divided into three stages: (I) the relaxing region of helium nano-bubbles below the free surface; (II) the escaping region of helium nano-bubbles due to over-pressurization inside them; (III) the stable region by the end of helium nano-bubbles releasing completely. Figure 2 shows the different evolution stages for the releasing process of helium nano-bubble as a function of the running time. In the relaxing region, the number of helium atoms inside the bubble keeps constant, but the bubble shape changes to varying degrees at different parameters, such as crystallographic orientation, temperature, and helium-to-vacancy ratio. In the escape region, the helium bubble can rapidly release in order that the whole system can keep the equilibrium state. The results show that the rapidest velocity of the released atoms is in the $[001]$ direction, and then in the $[1-10]$ direction, and finally in the $[111]$ direction. Actually, due to the different atomic arranges in different crystallographic orientations, the inner pressure of helium nano-bubble has difference, which leads to different escaping velocities of helium atom inside the bubble. The main escaping time is in the range of 0–10.0 ps. After 10.0 ps running time, the simulated box with the helium bubble has nearly finished from the relaxing process, the escaping process to the stable process. The dependence of the residuary helium atoms inside the simulation box is on the different conditions, such as the temperature and the inside stress of the helium bubble. A helium-bubble-free zone near the surface is found experimentally[34] and theoretically.[35] The similar phenomenon about the helium nano-bubble releasing has also been observed in our atomic-scale simulations. The zone between the bottom of helium nano-bubble and the surface is called "denuded zone", away from which the helium nano-bubble is retained in bulk, whereas the bubble will expand rapidly and release spontaneously as long as the bubble is within the zone. To obtain the helium nano-bubble escaping process from the surface, we fully make the bubble within the denuded zone and finally there is no helium atom trapped in the bubble. This suggests that the helium nano-bubble is unstable inside the denuded zone.

The helium-to-vacancy ratios also have a great influence on the helium nano-bubble escaping near the surface. With the helium-to-vacancy ratio increasing, the inside pressure of the helium nano-bubble increases. As the pressure passes the limitation, the helium nano-bubble starts to escape toward the surface. Here, we only considered four helium-to-vacancy ratios, such as $1:0$, $1:1$, $2:1$, and $3:1$. Figure 3 shows the dependence of the number of released helium atoms on the time for three free surfaces. At different He-to-vacancy ratios, the helium nano-bubble releasing process can also be divided into three regions. The first region is the relaxing process, and the second region is the releasing process, and the third region is the stable process. As examples, in the relaxing process, the number of helium atoms inside the bubble nearly keeps constant and the running time is around 1.5 ps. In the releasing process, the helium atoms rapidly escape from near surface by the "open" atomic channels. As the helium-to-vacancy ratio increases, the number of released helium atoms increases for the $Z[001]$ free surface. For the $Z[1-10]$ and $Z[111]$ two free surfaces, as the helium-to-vacancy ratio increases, the releasing helium atoms have some difference due to the surface configurations. In the stable process, as the helium-to-vacancy ratio increases, the number of releasing helium atoms increases accordingly. When the helium-to-vacancy ratio is $1:1$, due to the pressure inside the nano-bubble not being high enough, the helium atoms do not completely release from the free surfaces $Z[001]$ and $Z[111]$, respectively. This indicated that the crystallographic orientation and the pressure within the helium nano-bubble likely have a large influence on the denuded zone, which need to be further studied.

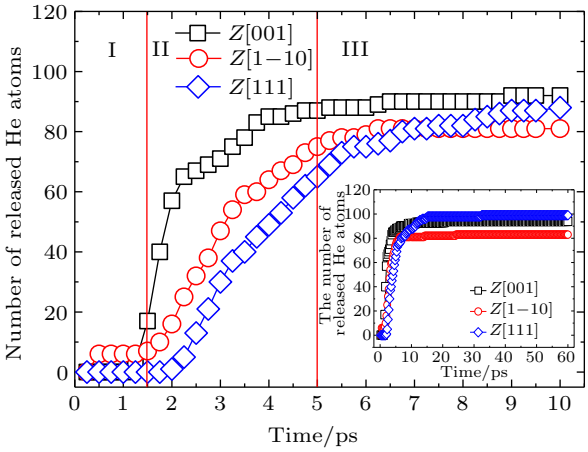


Fig. 2. (color online) The number of released He atoms as a function of the simulation time for different orientations with He-to-vacancy ratio 2 : 1 at 300 K in three regions: (I) the relaxing process; (II) the escaping process; (III) the stable process.

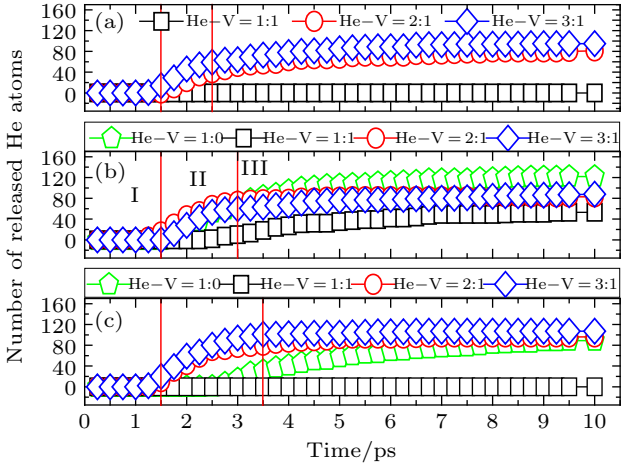


Fig. 3. (color online) The number of released He atoms as a function of the simulation time at 300 K with different orientations: (a) $Z[001]$; (b) $Z[1-10]$; (c) $Z[111]$ with the three regions: (I) the relaxing process; (II) the escaping process; (III) the stable process.

3.2. Dynamic process of helium nano-bubble release

The releasing process of the helium nano-bubble is a dynamics balance, which can reflect the channel formation connecting the helium nano-bubble to the near surface, then the helium atoms will easily escape from the matrix along this channel one by one or in the forms of smaller helium clusters until the new balance is built again. Thus, the formation of the channels and surface cavity is a great strategic point, which can accelerate the helium release from the near surface region.

Figure 4 presents the micro-process for the helium atom releasing from the near surface during the 250 ps. Here, we only show the case for the crystallographic orientation $Z[001]$ and He-to-vacancy is 3 : 1 at 300 K. Helium nano-bubble is located at different depths, H, from the Ni matrix surface, in which H will be adjusted according to the different crystallographic orientations, temperatures and He-to-vacancy ratios, in order to finish the escaping process of helium nano-bubble from near surface. The transformation of helium nano-bubble's shapes and morphology and reconstruction of surface as a function of running time are shown in Fig. 4. In the initial stage, the configuration of helium nano-bubble is approximately spherical and it can maintain a symmetric structure, similar to its initial configuration, which is marked by a as the time is 0.25 ps, and the interface between the nano-bubble and nickel atoms is pliable. With the running time increasing, the shape of helium nano-bubble starts to distort, and it is obviously elongated toward the surface, which is mainly due to the common influence of the inner pressure from nano-bubble and free surface. Once the balance between the internal pressure of the nano-bubble and the surface strain is broken and the channel is built, then helium atoms suddenly escape from the matrix surface along with the strong surface deformation, as shown labelled by b and c for $t = 1.00$ ps and 2.50 ps. It is of great interest to note that, when a majority of helium atoms escape from the surface, the residual helium atoms get together again and the surface is reconstructed, such as d for $t = 7.50$ ps. The morphology of the surface becomes much flatter than the one of the releasing process. It seems that the channels opened previously are shut down, the helium atoms are put inside the matrix, and the surface atoms repair exactly right. After that, the helium atoms continue to look for new channels in order to escape from the surface. During this period, the helium atoms try to burst through matrix atoms to form a new channel for releasing over and over again. Until the running time is over, the whole helium atoms have escaped from the matrix successfully for $t = 250.00$ ps. However, in this called "open"–"close"–"open"–"close" channel loop, after the first close escaping channel, residuary helium atoms will undergo much more time to search for new path. We also observed that only two or three helium atoms still quickly move inside the void to look for the way out for a long time. The surface presents multi-layers like "atomic islands", which appears after helium atoms releasing for the first time and keeps reconstruction in the complete process, like Figs. 4(d)–4(l) It is indicated that the channel is very critical for the atom escaping and its formation mechanism still needs a great deal of effort of further study.

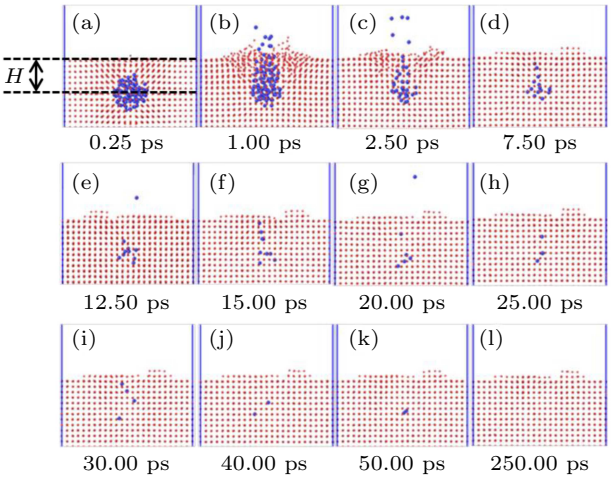


Fig. 4. (color online) The morphology of helium nanobubble releasing near the nickel surface as a function of the simulation time at He-to-vacancy ratio 3 : 1 for $Z[001]$ crystal orientation at 300 K. The red balls represent the nickel atoms and the blue balls represent the helium atoms. (a) 0.25 ps, (b) 1.00 ps, (c) 2.50 ps, (d) 7.50 ps, (e) 12.50 ps, (f) 15.00 ps, (g) 20.00 ps, (h) 25.00 ps, (i) 30.00 ps, (j) 40.00 ps, (k) 50.00 ps, and (l) 250.00 ps.

Moreover, due to the options of different parameters, such as He-to-vacancy ratio, temperature and crystallographic orientations, etc., some helium atoms are detained, which is not shown here. In particular, the crystallographic orientations have great effect on the nano-bubble bursting. Parish *et al.*[36] have investigated that the normal-direction crystallographic orientation of the underlying grain controls the growth morphology by SEM observation. They pointed out that grain formed pyramids near-$\langle 001\rangle\|$ normal direction (ND) formed wavy and stepped structures near-$\langle 114\rangle$ to $\langle 112\rangle\|$ ND, and remained smooth near-$\langle 103\rangle\|$ ND. For the crystallographic orientations, such as $Z[1-10]$ and $Z[111]$, the surface morphology also transformed from the smooth free surface to the "pyramid" style or layer-by-layer or stepped style, or even the mixed style (both of them) after nano-bubble bursting and escaping from the surface, which was similar to the case in $Z[001]$ crystallographic orientation. This suggested that the crystallographic orientation will directly influence the surface morphology during the nano-bubble bursting and escaping process.

Here, we consider the influence of crystallographic orientation and He-to-vacancy ratios at 500 K. The release rate also appears to have three stages: (I) the accelerating release rate from 0 to around 3.0 ps, which corresponds to the high pressure inside helium nano-bubbles; (II) the decelerating release rate from 3.0 ps to 10.0 ps, which may be associated with the decrease of the number of helium atoms, and (III) the constant process, relatively a low release rate, which is not shown here.

For different crystallographic orientations, the maximum released rate is found along $Z[001]$, then $Z[1-10]$ and $Z[111]$, as shown in Fig. 5, which is mainly due to the arrangement of surface atoms. Furthermore, for the He-to-vacancy ratios, the curve profile of the release rate as a function of running time is nearly similar. It suggests that the release rate for the high pressure inside the nano-bubble will also undergo the same three stages.

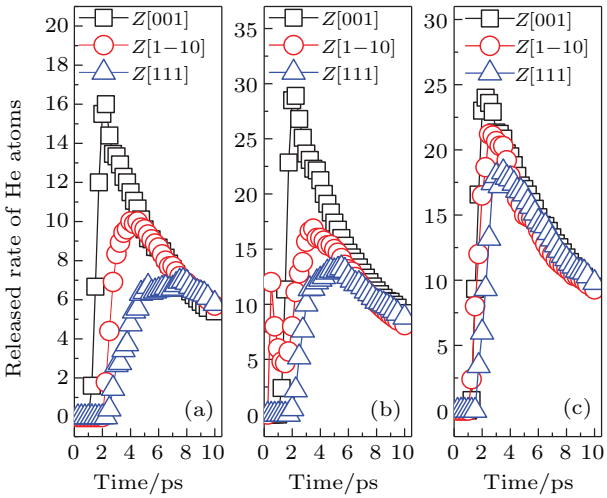


Fig. 5. (color online) Released rate of He atoms as a function of the simulation time at 500 K for different orientations with He-to-vacancy ratios: (a) 1 : 1; (b) 2 : 1; (c) 3 : 1.

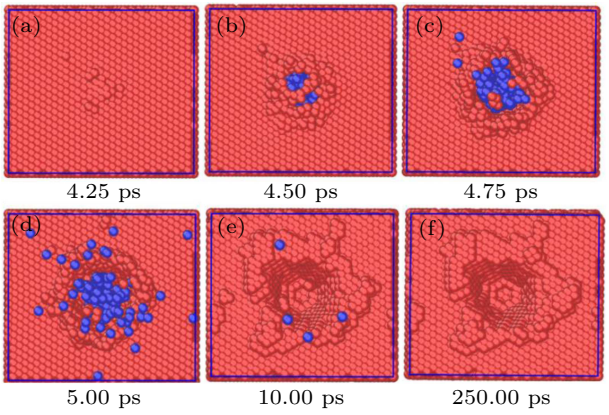


Fig. 6. (color online) The morphology of helium nano-bubble releasing near the nickel surface as a function of the simulation time at He-to-vacancy ratio 3 : 1 for $Z[111]$ crystallographic orientation at 300 K. (a) 4.25 ps, (b) 4.50 ps, (c) 4.75 ps, (d) 5.00 ps, (e) 10.00 ps, (d) 250.00 ps.

The different configurations of the surface layers with some critical running time are also shown in Fig. 6. At $t = 4.25$ ps, there appears a hump on the $Z[111]$ surface, which is the embryo of the cavity for helium nano-bubble escaping from the surface, which can explain the blistering phenomenon observed experimentally in Ref. [4] microscopically, which can also be adopted to illuminate the appearance of blisters coincided with the gas release from the surface by Erents *et al.*[37] As the running time is 4.50 ps, the cavity in the early stage has been formed in order that helium atoms begin to burst out, leaving several areas of damage to the surface. The helium atoms totally escape from the surface until the large cavity only remains on the surface with the process of reconstruction. It is noted that in the whole process, the matrix atom is not away from the surface, due to the fact that the inside pressure of the nano-bubble is not high enough. By comparison among crystallographic orientations $Z[001]$, $Z[1-10]$, and $Z[111]$, the common feature is the void formation and surface reconstruction. However, due to different atomic arrangements along different crystallographic orientations, the surface morphology, channel formation and nano-bubble structures also present great diversity, which needs to be strongly concerned in the further step.

3.3. Pressure evolution

Due to the helium atoms added into the system during the simulation only for one time, the bubble pressure is triggered to increase above equilibrium, which develops compressive strain in the surrounding nickel matrix. Under overpressure conditions within helium nano-bubbles, the bubble center of mass is relatively shallow compared to its size, the bubbles feel an attraction from free surface and tend to escape toward it along the direction of least resistance. With the bubble overpressurization, pressure relief processes occur to relieve the internal pressure through prismatic interstitial loop-punching or by fracturing or deforming the surface ligament above the bubbles to the point of rupture, resulting in helium release. In some configurations, particularly when the bubbles are small and the ligament is thin. The pressure will simply increase until the ligament breaks without prior deformation of the nickel surface. In other cases, the bubble can increase the volume to reduce pressure. In the paper, we only consider the contribution of virial stress to the stress tensor for the whole simulation box. The macroscopic pressure P of a set of interacting atoms contained in a volume V can be derived in a number of methods, such as continuum mechanics, classical mechanics, and statistical mechanics.[38,39] All of these derivations result in the following well-established relationship:

$$P = \frac{Nk_{\mathrm{B}}T}{V} + \frac{\langle W \rangle}{3V}, \tag{1}$$

$$W(\boldsymbol{r}^N) = -3V\frac{\mathrm{d}U}{\mathrm{d}V}, \tag{2}$$

where N is the number of atoms in the simulation box, T is the temperature, k_{B} is Boltzmann's constant, and V is the volume of the simulation box, and the angle brackets in the second term denote an appropriate ensemble average of the internal virial W, which represents the contribution to the total virial due to forces acting between the atoms. In Eq. (2), U is the potential energy due to interactions between the atoms. The virial, like the forces and potential energy, depends only on the instantaneous atom positions $\boldsymbol{r}^N = \boldsymbol{r}_1, \ldots, \boldsymbol{r}_N$ and the interactions between them.

Figure 7 provides examples of how stress changes to understand the bubble evolution. The stress discussed in this work is a negative pressure (P) accordingly. Here, we show the influence of different He-to-vacancy ratios (1 : 0, 1 : 1, 2 : 1, and 3 : 1) on the stress for the whole simulation cell. It is obvious that the curve presents the high symmetric oscillation along the XY and Z directions, respectively. The amplitude is three times more in the Z direction than in the XY plane, due to the releasing surface along Z direction. As the He-to-vacancy ratio increases, the symmetry of stress is damaged and the peak broadening becomes narrow. The running time increases, the stress becomes small, due to the pressure decreases inside the nano-bubble. Moreover, in our calculations, the stress as a function of temperature is also investigated. With the time running, the stress becomes decreased slowly and, as temperature increases, the stress also presents as increasing, as shown in Fig. 8. This indicates that the releasing phenomenon of helium atoms is a looking for the channels, then diffusion and escape process and it can be repeated for more than once.

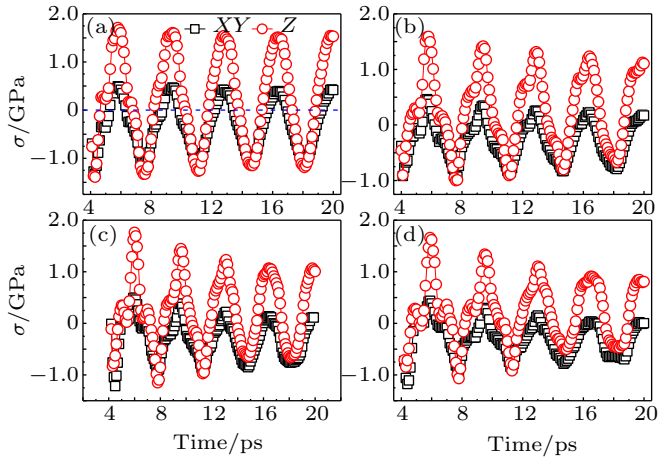


Fig. 7. (color online) The stress variant as a function of the simulation time at 300 K for Z[111] orientation with He-to-vacancy ratios: (a) 1 : 0; (b) 1 : 1; (c) 2 : 1; (d) 3 : 1.

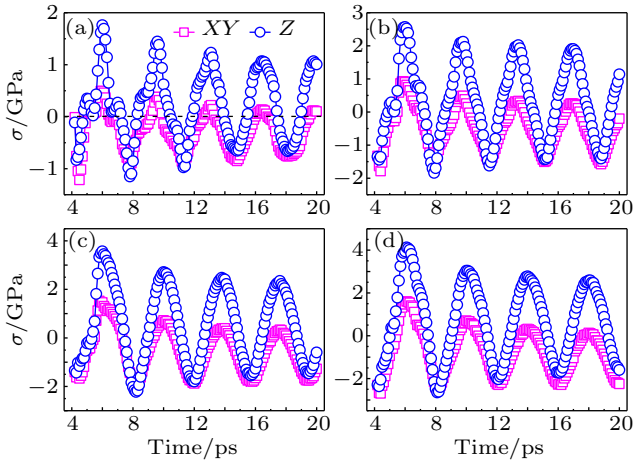


Fig. 8. (color online) The stress variant as a function of the simulation time at He-to-vacancy ratio 2:1 for Z[111] orientation at different temperatures: (a) 300 K; (b) 500 K; (c) 800 K; (d) 1000 K.

4. Conclusion

The microscopic mechanism of helium release from a nickel near surface is investigated using MD method. A denuded zone has been observed in the modeling simulation, which can support the experimental observation. The channel usually needs to undergo "open" and "close" processes more than once during the releasing process. The present simulations provide a physical explanation for why the helium is released only from the near-surface region rather than through bulk diffusion. The helium release is an instantaneous process, with the helium erupting from the surface, creating surface deformation and the nucleation of a cavity on the surface. The cavity formation can further accelerate the helium release from the surface. This model is tested to compare with the experimental result from Hastelloy N alloys implanted by helium ions and satisfactory agreement is obtained. In addition, the study demonstrates that atomic-level simulations provide an important method to understand the dynamic process of helium release as well as determining the effects of the actual material microstructures on helium behavior in nuclear materials.

Acknowledgment

The Shanghai Supercomputing Center and Lanzhou Supercomputing Center are acknowledged for allocation of computing time.

References

[1] Bloom E E, Busby J T, Duty C E, Maziasz P J, McGreevy T E, Nelson B E, Pint B A, Tortorelli P F and Zinkle S J 2007 *J. Nucl. Mater.* **367** 1
[2] Zinkle S J and Busby J T 2009 *Mater. Today* **12** 12
[3] McCoy Jr H E 1978 *Status of Materials Development for Molten Salt Reactors* (United States) pp. 1–40
[4] Liu M 2013 *Investigation on Corrosion Behavior and Irradiation Performance of the Structural Material (Hastelloy N Alloy) in Molten Salt Reactor* (Doctoral Dissertation, Shanghai Institute of Applied Physics) pp. 75–87
[5] Stoller R E and Odette G R 1988 *J. Nucl. Mater.* **154** 286
[6] Lewis M B and Farrell K 1986 *Nucl. Instrum. Methods Phys. Res. B* **16** 163
[7] Bloom E E, Busby J T, Duty C E, Maziasz P J, McGreevy T E, Nelson B E, Pint B A, Tortorelli P F and Zinkle S J 2007 *J. Nucl. Mater.* **367** 1
[8] Evans J H and van Veen A 1996 *J. Nucl. Mater.* **233–237** 1179
[9] Donald F C 2005 *Fus. Sci. Tech.* **48** 539
[10] Morishita K 2007 *Phil. Mag.* **87** 1139
[11] Kajita S, Daeki T, Yoshida N, Ohno N and Iwamae A 2010 *Appl. Phys. Expr.* **3** 085204
[12] Cipiti B B and Kulcinski G L 2005 *J. Nucl. Mater.* **347** 298
[13] Zenobia S J and Kulcinski G L 2009 *Fus. Sci. Tech.* **56** 352
[14] Sefta F, Juslin N and Wirth B D 2013 *J. Appl. Phys.* **114** 243518
[15] Sefta F, Hammond K D, Juslin N and Wirth B D 2013 *Nucl. Fus.* **53** 073015
[16] Zhang B L, Wang J, Li M and Hou Q 2013 *J. Nucl. Mater.* **438** 178
[17] Ohno N, Hirahata Y, Yamagiwa M, Kajita S, Takagi M, Yoshida N, Yoshihara R, Tokunaga T and Tokitani M 2013 *J. Nucl. Mater.* **438** 5879
[18] El-Atwani O, Hinks J A, Greaves G, Gonderman S, Qiu T, Efe M and Allain J P 2015 *Sci. Rep.* **4** 4716
[19] http://lammps.sandia.gov/
[20] Daw M S and Baskes M I 1984 *Phys. Rev. B* **29** 6443
[21] Baskes M I 1992 *Phys. Rev. B* **46** 2727

[22] Daven D M, Tit N, Morris J R and Ho K M 1996 *Chem. Phys. Lett.* **256** 195
[23] Deng H, Hu W, Shu X and Zhang B 2003 *Surf. Sci.* **543** 95
[24] Yang J, Hu W, Deng H and Zhao D 2004 *Surf. Sci.* **572** 439
[25] Hu W, Zhang B, Huang B, Gao F and Bacon D J 2001 *J. Phys.: Conden. Matter* **13** 1193
[26] Hu W, Deng H, Yuan X and Fukumoto M 2003 *Euro. Phys. J. B* **34** 429
[27] Hu W, Shu X and Zhang B 2002 *Comput. Mater. Sci.* **23** 175
[28] Hu W and Fukumoto M 2002 *Modell. Simula. Mater. Sci.* **10** 707
[29] Johnson R A 1990 *Phys. Rev. B* **41** 9717
[30] Baskes M I and Melius C F 1979 *Phys. Rev. B* **20** 3197
[31] Johnson R A 1973 *J. Phys. F: Metal Phys.* **3** 295
[32] Xia J X, Hu W Y, Yang J Y and Ao B Y 2006 *Phys. Stat. Soli. B* **243** 579
[33] Nosé S 1991 *Prog. Theor. Phys. Suppl.* **103** 1
[34] Snow C S and Brewer L N 2008 *J. Nucl. Mater.* **374** 147
[35] Gowgill D F 2005 *Fus. Sci. Tech.* **48** 539
[36] Parish C M, Hijazi H, Meyer H M and Meyer F W 2014 *Acta Mater.* **62** 173
[37] Adda Y, Beyeler M and Brebec G 1975 *Thin Solid Films* **25** 107
[38] Hummer G, Lawrence R P and Angel E G 1998 *J. Chem. Phys.* **109** 7885
[39] Hünenberger P H 2002 *J. Chem. Phys.* **116** 6880